Few-photon transport in low-dimensional systems

Paolo Longo[*]
Institut für Theoretische Festkörperphysik, Karlsruhe Institute of Technology, Wolfgang-Gaede-Str. 1, D-76131 Karlsruhe, Germany

Peter Schmitteckert[†]
Institute of Nanotechnology, Karlsruhe Institute of Technology, D-76344 Eggenstein-Leopoldshafen, Germany

Kurt Busch[‡]
Institut für Theoretische Festkörperphysik and DFG-Center for Functional Nanostructures, Karlsruhe Institute of Technology, Wolfgang-Gaede-Str. 1, D-76131 Karlsruhe, Germany

(Received 22 February 2011; published 22 June 2011)

We analyze the role of quantum interference effects induced by an embedded two-level system on the photon transport properties in waveguiding structures that exhibit cutoffs (band edges) in their dispersion relation. In particular, we demonstrate that these systems invariably exhibit single-particle photon-atom bound states and strong effective nonlinear responses on the few-photon level. Based on this, we find that the properties of these photon-atom bound states may be tuned via the underlying dispersion relation and that their occupation can be controlled via multiparticle scattering processes. This opens an interesting route for controlling photon transport properties in a number of solid-state-based quantum optical systems and the realization of corresponding functional elements and devices.

DOI: 10.1103/PhysRevA.83.063828 PACS number(s): 42.50.Nn, 42.50.Gy, 42.70.Qs

I. INTRODUCTION

Advances in micro- and nanofabrication technologies combined with a significantly improved understanding of the underlying physical mechanisms form the basis of most of the recent progress in quantum photonics as well as in cavity and circuit QED.

In the area of quantum photonics, high-quality single-photon sources have been developed and can readily be integrated with conventional waveguiding elements [1–6] (for an overview we refer to Ref. [7]). In addition, several types of integrated optical resonators with very high quality factors such as ring resonators, disk resonators, and photonic crystal resonators have become available and may be arranged into various forms of arrays [8–10]. When these waveguiding structures and resonators are equipped with judiciously placed quantum-optical emitters such as quantum dots and nitrogen-vacancy centers in nanodiamond crystals, complex solid-state-based quantum optical functional elements may be realized. Consequently, much of the ongoing work aims at precisely positioning these quantum emitters within artificially structured optical materials [11–17].

Similarly, in cavity and circuit QED, high-quality superconducting wave guides and cavities [18], strong coupling of single photons to superconducting qubits [19], and Fock states [20] have been realized for microwave photons. In addition, these waveguides and cavities may be combined with Josephson junctions and several of these compound elements may be arranged to form left- and right-handed transmission lines that exhibit tunable dispersion relations [21]. Moreover, suitably engineered Josephson junctions realize few-level quantum systems for microwave photons whose coupling strength to the radiation field can be tuned to values that are simply not available in traditional quantum-optical systems at optical frequencies [22].

Despite the apparent disparity in operation wavelengths and underlying physical system, the common goal of all the above approaches is the realization of integrated quantum optical devices that operate in the few-photon regime. This includes but is not limited to the more specific goals of efficient generation and detection of single photons (or even plasmons [17]), the realization and control of effective photon-photon interaction processes, the generation and control of photon entanglement, and—based on these fundamental building blocks—the realization of complex quantum-optical functional elements and devices [23]. As most of such high-quality samples and systems have become available only recently, there exists a rather limited number of theoretical works that explore the potential of such systems with regards to modifying light-matter interaction and its utilization for realizing and controlling the above effective light-light interaction. Similar to the early works by Fano, which have been concerned with a discrete (electronic) state that interacts coherently with a continuum of (electronic) states [24], we may expect interesting physics to occur in the photonic case as well. Obviously, the details will depend on the emitter, its interaction with the continuum and—quite important for the photonic case—the structure of the continuum itself.

In the present context, this suggests that low-dimensional waveguiding systems with embedded quantum impurities facilitate enhanced quantum interference effects for single- and few-photon processes. On the one-photon level, a single two-level system (TLS) realizes an energy-dependent mirror [25–28]. Furthermore, and in contrast to the classical π-pulse scenario (which only puts constraints on the pulse area), at least for a linear dispersion relation without band edges, there

[*]paolo.longo@kit.edu
[†]peter.schmitteckert@kit.edu
[‡]kurt.busch@kit.edu

exists a unique pulse shape that leads to a (momentarily) full inversion of the TLS [29].

A single TLS embedded into a one-dimensional waveguide leads to an effective photon-photon interaction. According to Refs. [30–32], it may even lead to photon-photon bound states in the case of two or more photons. Both effects are of direct relevance for the generation and control of photon-photon entanglement. In addition, realistic waveguiding systems feature cut-offs or band edges in their dispersion relations, and this leads to the formation of single-particle bound states of the combined TLS + waveguide system [32,33]. These single-particle states can only be accessed via nonlinear multiparticle processes and may be utilized for the efficient and robust trapping of radiation with applications for novel detectors and quantum logic functional elements [33].

Embedding a three-level emitter into a one-dimensional waveguiding system adds yet another twist, as now an external classical driving field allows for additional control mechanisms. For instance, in the V configuration the state of the emitter can be switched deterministically by the driving field via Raman scattering. In essence, this realizes a single-photon transistor [34]. Arrays of so-called Jaynes-Cummings cavities represent a further promising class of such solid-state-based quantum-optical systems. Here, a set of ordinary resonators, each equipped with a single TLS that interacts with a single-resonator mode, are coupled together to form an artificial optical material where concepts analogous to classical wave propagation in photonic crystals and metamaterials have been studied on the one-photon level [35].

With the exception of a few works on the one-photon case [27,29] and our work on the few-photon transport [33], all of the above calculations have been carried out in the stationary regime. Specifically, the more challenging few-photon case has been addressed with sophisticated Bethe-Ansatz [30,31] and Lehmann-Symanzik-Zimmermann reduction techniques [32] that allow the determination of the corresponding scattering matrices. However, as these field-theoretical approaches employ linearized dispersion relations without band edges, they do not contain the physics of the photon-atom-bound state described above.

In this paper, we extend our earlier study of few-photon transport in low-dimensional waveguiding systems with an embedded TLS [33] and provide further results regarding interaction-induced radiation trapping via photon-atom bound states, the underlying physical mechanisms, and its applications. To facilitate this, we briefly review in Sec. II the details of the model and our computational framework. We discuss the single-particle photon-atom bound states and radiation trapping for different types of dispersion relations in Secs. III and IV, respectively. In Sec. V, we provide a detailed analysis of the underlying nonlinear multiparticle scattering processes, and in Sec. VI we analyze the redistribution of momenta during such scattering processes that are constrained by total energy conservation.

II. FUNDAMENTALS

A. The Model

We start with the foundation for all theoretical considerations in this paper, which is given by the celebrated Dicke-Hamiltonian [36]. This represents a multimode generalization of the well-known Jaynes-Cummings model [37] and, therefore, constitutes a generic description of fully quantum-mechanical light-matter interaction in the sense discussed above. For modeling the interplay of one photonic band with a single TLS, we write the Hamiltonian in the rotating-wave approximation as

$$\hat{H} = \sum_k \epsilon_k\, a_k^\dagger\, a_k + \frac{\Omega}{2}\sigma_z + \sum_k (V_k\, \sigma^+\, a_k + V_k^*\, \sigma^-\, a_k^\dagger). \tag{1}$$

Here, $a_k^\dagger$ and a_k are bosonic creation and annihilation operators for photons with wavenumber k, ϵ_k denotes the photonic dispersion relation of the underlying waveguiding system, and Ω represents the atomic transition energy. The usual Pauli operators σ_z and $\sigma^\pm$ describe, respectively, the atomic inversion and the raising/lowering of the atomic state. In general, the atom-field coupling strength V_k depends on the photonic dispersion, the atomic dipole matrix element, and the quantization volume. As we will, in the following, apply certain simplifications to the Hamiltonian (1), we will from now on also disregard the explicit momentum-dependence of the coupling constants V_k. Finally, we restrict our investigations to the case of a single band of effectively one-dimensional photonic systems. Such systems frequently occur in experimental settings, notably in the context of photonic crystal waveguides and superconducting transmission lines, and their reduced dimensionality leads to rather strong quantum interference processes. Our computational framework, which we present below, does not rely on the above simplifications and can accommodate several bands, momentum-dependent coupling constants, and higher-dimensional systems. For instance, an approach based on photonic Wannier functions [38,39] provides a quantitative tight-binding-like real-space description [cf., Eqs. (3), (4), and (5) below]. Nevertheless, the above simplifications allow for a much more transparent discussion of the relevant physics.

In the context of transport calculations, we find it useful to work with an equivalent real-space formulation of the problem. By applying a lattice Fourier transform,

$$a_k^\dagger = \frac{1}{\sqrt{N}} \sum_{j=1}^{N} e^{\imath k j a} a_j^\dagger, \tag{2}$$

the Dicke-Hamiltonian (1) takes the form

$$\hat{H} = \sum_{j \neq j'} (J_{jj'}\, a_j^\dagger\, a_{j'} + \text{H.c.}) + \frac{\Omega}{2}\sigma_z + \sum_j (G_j\, \sigma^+\, a_j + \text{H.c.}). \tag{3}$$

In the above expression, we have introduced the hopping elements $J_{jj'}$ and the Fourier transform of the atom-field coupling G_j:

$$J_{jj'} = \frac{1}{N} \sum_k \epsilon_k e^{\imath k a (j-j')} \equiv J_{j-j'}, \tag{4}$$

$$G_j = \frac{1}{\sqrt{N}} \sum_k V_k e^{-\imath k a j}. \tag{5}$$

Furthermore, N denotes the number of modes (number of wave numbers k) in the momentum-space formulation. This number is identical to the number of lattice sites in the real-space formulation. In addition, a stands for the lattice constant so that the system's total length is $L = Na$. Note, the lattice constant a cannot be confused with the annihilation operators in real or momentum space, a_k and a_x, as the latter always carry an appropriate index. For the above-mentioned simplification of a momentum-independent coupling $V_k = V/\sqrt{N}$, the atom-field coupling becomes local in real space, i.e., we have $G_j = V\delta_{x_0 j}$, where x_0 is the position of the TLS. By additionally limiting the hopping elements to be nonvanishing for nearest neighbors only, $J_{jj'} = -J(\delta_{jj'+1} + \delta_{jj'-1})$, and by applying hard-wall boundary conditions at the ends of the chain, the Hamiltonian (3) finally takes the form of a bosonic tight-binding model with a fermionic impurity that is side-coupled to the lattice site x_0:

$$\hat{H} = -J\sum_{x=1}^{N-1}(a_{x+1}^\dagger a_x + a_x^\dagger a_{x+1}) + \frac{\Omega}{2}\sigma_z + V(\sigma^+ a_{x_0} + \sigma^- a_{x_0}^\dagger). \tag{6}$$

If not explicitly stated otherwise, we will, in the following, employ the above tight-binding formulation (6), which yields a cosine-shaped dispersion relation $\epsilon_k = -2J\cos(ka)$ (cf., Fig. 1). In order to obtain further insight into the problem, we provide an equivalent form of the Hamiltonian [Eq. (6)], which reads

$$\hat{H} = -J\sum_{x=1}^{N-1}(a_x^\dagger a_{x+1} + a_{x+1}^\dagger a_x) + \Omega b^\dagger b + U b^\dagger b(b^\dagger b - 1) + V\left(a_{x_0} b^\dagger + a_{x_0}^\dagger b\right). \tag{7}$$

Here, we have replaced the atomic operators σ_z and $\sigma^\pm$ by appropriate combinations of bosonic creation and annihilation operators, $b^\dagger$ and b, that belong to an additional bosonic site with on-site energy Ω that side-couples (via the coupling constant V) to the waveguide. More precisely, we have replaced the free-atom part of the Hamiltonian according to $(\Omega/2)\sigma_z \to \Omega b^\dagger b + U b^\dagger b(b^\dagger b - 1)$, so that in the limit $U \to \infty$ the atom can at most absorb one photon. In other words, sending $U \to \infty$ in Eq. (7) shifts all except the two lowest-lying levels of the additional bosonic site to infinity

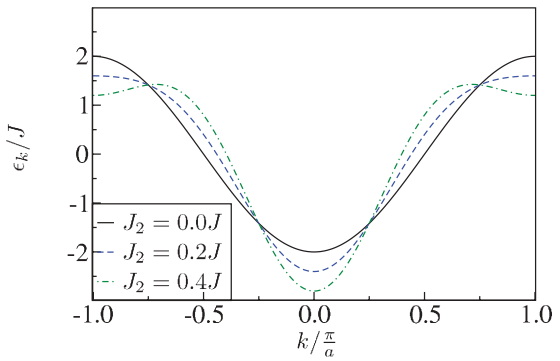

FIG. 1. (Color online) Dispersion relations $\epsilon_k = -2J\cos(ka) - 2J_2\cos(2ka)$ for tight-binding models with next-nearest-neighbor hopping term J_2.

so that we can identify the original atomic ground state with the case of zero bosons on this additional site and the original excited state of the atom with the case of one boson on this additional site. States with more than one boson on this additional site are irrelevant, i.e., we recover a true TLS description and there is neither a numerical nor a physical difference between Hamiltonian Eq. (6) and Hamiltonian Eq. (7).

Nevertheless, from the Hamiltonian Eq. (7) we immediately deduce that the corresponding transport properties will strongly depend on the particle (or excitation) number because the term $Ub^\dagger b(b^\dagger b - 1)$ depends in a nonlinear way on $b^\dagger b$. In turn, this has the immediate consequence that few- or many-body eigenfunctions of the system are not just direct products of corresponding single-particle eigenstates. Therefore, an analytical treatment of the problem turns out to be very challenging [30–32]. On the other hand, the form of the Hamiltonian Eq. (7) immediately suggests that certain numerical or analytical techniques that have been developed for correlated electron systems may be adapted to this case.

B. Initial States, Time Evolution, and Observables

In the context of dynamical transport calculations, we evolve quantum states in time according to

$$|\Psi(t)\rangle = e^{-\frac{i}{\hbar}\hat{H}\cdot(t-t_0)}|\Psi(t_0)\rangle, \tag{8}$$

where $|\Psi(t)\rangle$ stands for the full-state vector of radiation field plus TLS. The time evolution is carried out using Krylov-subspace-based operator-exponential techniques [40–42,44]. To this end, it is helpful to note that the (equivalent) Hamiltonians [Eqs. (6) and (7)] conserve the total number of excitations so that we can, depending on the initial condition $|\Psi(t_0)\rangle$, restrict the simulations to the corresponding sector of the Hilbert space [27]. As a result, we can evolve Eq. (8) by means of exact numerics for the case of one or two particles. As the dimension of the Hilbert space grows rapidly with the number of particles, we have to employ density-matrix-renormalization-group methods (DMRG) [43] in the case of more than two particles. Within the applied time-dependent DMRG scheme we perform the full time evolution at each DMRG step [44,45]. The local vector space is restricted to the total number of photons of the complete system. Note that one could enhance resolution in energy space by applying discretization schemes as explained in Ref. [46].

An initial condition in the m-particle sector of the Hilbert space that contains m photons has the general form

$$|\Psi(t_0)\rangle = \sum_{x_1=1}^{N}\cdots\sum_{x_m=1}^{N}\Phi_{x_1,\ldots,x_m}a_{x_1}^\dagger\ldots a_{x_m}^\dagger|0,\downarrow\rangle, \tag{9}$$

where $|0,\downarrow\rangle$ denotes the product state of the vacuum state of the radiation field (no photon on any lattice site) and the atom being in its ground state (or, equivalently zero bosons on the additional bosonic site). Due to the bosonic nature of photons, the many-body wave function $\Phi_{x_1,\ldots,x_m}$ has to be totally symmetric with respect to permutations of the coordinate variables and, therefore, can be written as

$$\Phi_{x_1,\ldots,x_m} = \frac{1}{\sqrt{m!}}\hat{\mathcal{S}}_{x_1,\ldots,x_m}\varphi_{x_1}^{k_0^{(1)},x_c^{(1)},s^{(1)}}\ldots\varphi_{x_m}^{k_0^{(m)},x_c^{(m)},s^{(m)}}. \tag{10}$$

Here, $\hat{\mathcal{S}}_{x_1,\ldots,x_m}$ denotes the symmetrization operator that executes a sum over all permutations of coordinate variables, and $\varphi_{x_j}^{k^{(l)},x_c^{(l)},s^{(l)}}$ stands for a single-particle Gaussian wave function with carrier wavenumber $k^{(l)}$, center $x_c^{(l)}$, and width $s^{(l)}$. For more details about simulation issues such as considerations regarding the finite system size, we refer the reader to our earlier work [27].

Having the full quantum state $|\Psi(t_0)\rangle$ of the combined waveguiding plus TLS system at our disposal, we can define the relevant physical quantities whose time evolutions we investigate in the subsequent sections. The transport process can be monitored in an intuitive way by examining the expectation values of the real-space occupation numbers

$$\langle n_x(t)\rangle = \langle\Psi(t)|a_x^\dagger a_x|\Psi(t)\rangle. \tag{11}$$

Together with the occupation of the excited atomic level, which can either be expressed through Pauli or (equivalently) through bosonic operators,

$$\langle n_b(t)\rangle = \langle(\sigma_z(t)+1)/2\rangle = \langle\Psi(t)|b^\dagger b|\Psi(t)\rangle, \tag{12}$$

we are able to obtain a nearly complete picture of the scattering of photon wave packets by the TLS. However, we find that Fourier transforms of the wave function amplitudes provide very useful further information by way of time-resolved momenta distributions. Specifically, for the case of a general two-photon state,

$$|\Psi\rangle = \sum_{x_1=1}^{N}\sum_{x_2=1}^{N}\Phi_{x_1,x_2}a_{x_1}^\dagger a_{x_2}^\dagger|0,\downarrow\rangle + \sum_{x=1}^{N} e_x a_x^\dagger|0,\uparrow\rangle, \tag{13}$$

the corresponding Fourier-transformed amplitudes for the atom in the ground and excited states (and correspondingly two and one photons in the waveguide), Φ_{k_1,k_2} and e_k, read as

$$\Phi_{k_1,k_2} = \frac{1}{\sqrt{N^2}}\sum_{x_1=1}^{N}\sum_{x_2=1}^{N} e^{\imath(k_1x_1+k_2x_2)}\Phi_{x_1,x_2}, \tag{14}$$

$$e_k = \frac{1}{\sqrt{N}}\sum_{x}^{N} e^{\imath kx}e_x. \tag{15}$$

Note that these amplitudes are time-dependent.

Finally, we define the units for the remainder of this work: We will express length, time, energy, and wavenumber, in units a (lattice constant), $\hbar/J$, J (the nearest-neighbor hopping element), and π/a, respectively.

III. PHOTON-ATOM BOUND STATES

Photon-atom bound states, i.e., mixed states of atomic and photonic excitations, are dressed (polaritonic) eigenstates of a system with discrete (atomic) levels that is coupled to a continuum of states (photonic band). This problem has attracted attention for a long time [24] and manifests itself in different contexts. For instance, photon-atom bound states play an important role when describing spontaneous emission in photonic bandgap media [47,48] or quantum-optical photon transport [32,33,49]. In this section, we would like (i) to demonstrate the existence of such bound states in a system that is described by the Hamiltonian Eq. (6) and (ii) to discuss their relevance for the photon transport in such systems.

In particular, Zhou *et al.* [26] have calculated the single-particle scattering eigenstates for the infinite system. These scattering states are sufficient to describe single-particle transport, but they do not form a complete basis of the single-particle Hilbert space. In order to obtain a complete basis, bound eigenstates with energies outside the range of the cosine-band have to be taken into account.

The corresponding eigenvalue problem $(\hat{H}-E)|\Psi\rangle = 0$ with a general state

$$|\Psi\rangle = \sum_x \varphi_x a_x^\dagger|0,\downarrow\rangle + e|0,\uparrow\rangle \tag{16}$$

in the single-particle subspace yields two coupled equations for the probability amplitudes φ_x and e, which can be combined to

$$-J(\varphi_{x+1}+\varphi_{x-1}) - \left(E+\frac{\Omega}{2}\right)\varphi_x + \frac{V^2}{E-(\Omega/2)}\varphi_{x_0}\delta_{xx_0} = 0. \tag{17}$$

Upon inserting an appropriate ansatz for bound states,

$$\varphi_x \propto e^{-\kappa|x-x_0|} \quad \text{with} \quad \mathrm{Re}(\kappa) > 0, \tag{18}$$

we obtain the quartic equation

$$\eta^4 + \frac{\Omega}{J}\eta^3 + \left(\frac{V}{J}\right)^2\eta^2 - \frac{\Omega}{J}\eta - 1 = 0 \tag{19}$$

for the variable $\eta \equiv \mathrm{e}^{-\kappa}$.

The polynomial Eq. (19) always has two physical solutions that satisfy $\mathrm{Re}(\kappa) > 0$ unless we take the limit $J \to \infty$, which corresponds to shifting the band edges energetically to $\pm\infty$. In this special case, none of the 4th-order roots of unity, $\eta^4 = 1$, represents a physical solution. This clearly highlights the role of band edges and, furthermore, explains why photon-atom bound states are removed from the physically accessible Hilbert space for linearized photonic dispersions without cut-off [25,30,31].

As mentioned above, dispersion relations other than the cosine dispersion can be included into our framework via long-range hopping terms that go beyond nearest-neighbor-hopping terms (see Fig. 1). In terms of the above discussion regarding the existence of photon-atom bound states, this leads to higher-order polynomials in η as compared to Eq. (19) so that analytic solutions become considerably more involved. Therefore, we demonstrate the existence of photon-atom bounds states in such systems in the next section with the help of our numerical approach (see also Refs. [32,47,50,51] for similar discussions). Clearly, as there is nothing special about a cosine-shaped dispersion relation, we expect that such single-particle bound states exist in any one-dimensional waveguiding system with a band edge or frequency cut-off that is side-coupled to a TLS. These bound states lead to interesting physical consequences [33] and in the following sections we provide further examples and details.

IV. RADIATION TRAPPING

The photon-atom bound states that we have introduced in the previous section are energetically outside the photonic

band and, therefore, cannot be accessed by a single particle with energy in the band, i.e., a photon that propagates in the waveguide. However, the local U term in the Hamiltonian Eq. (7) provides scattering processes between all single-particle eigenstates, including the bound state and, therefore, provides a physical mechanism for in-band particles to access the bound states via nonlinear multiparticle scattering processes.

In Ref. [33], we have determined the optimal parameters for the excitation of bound states for systems with nearest-neighbor hopping terms, i.e., for cosine-shaped dispersion relations. Here, we want to demonstrate that radiation trapping is a generic effect for systems with a band edge or a frequency cut-off. In Fig. 1, we display dispersion relations for systems with nearest- and next-nearest-neighbor hopping terms, where the strength of the next-nearest-neighbor hopping J_2 is varied. Next, we prepare as an initial condition a two-photon wave packet with identical photons [identical momenta, centers, and widths of the single-particle Gaussian wave functions in Eq. (10)] that is located sufficiently far away from the TLS, which is in its ground state. In addition, the momenta are selected such that the single-particle resonance criterion is satisfied, i.e., that the photon energy equals the atomic transition energy. Then, we let the wave packet propagate toward the TLS and investigate the interaction process by monitoring the TLS's excited-state population $\langle n_b(t)\rangle$. In Fig. 2, we depict the time evolution $\langle n_b(t)\rangle$ for the dispersion relations shown in Fig. 1. Once the two-photon wave packet reaches the TLS, part of the radiation is absorbed by the TLS and leads to a population of the excited state. In contrast to a one-photon interaction scenario, where only the scattering states are relevant for the scattering process [26,27], we now find the nonlinear scattering processes become effective. Therefore, bound states do play a role and an excitation of these bounds states becomes possible. After a certain interaction time, the photons propagate away from the TLS in the form of a transmitted and reflected wave packet. However, this implies

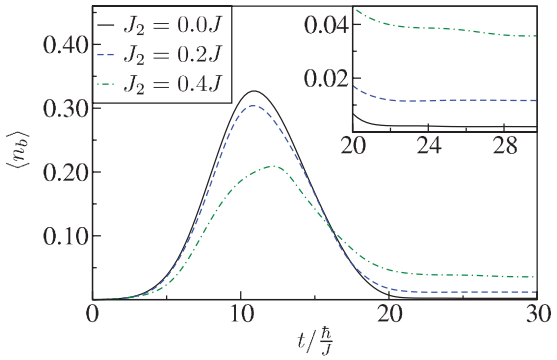

FIG. 2. (Color online) Time evolution of the occupation of the TLS's excited state $\langle n_b\rangle$ for an incoming two-photon wave packet and the dispersion relations depicted in Fig. 1. The parameters are (see text for details): $L = 99a$, $x_0 = 50$, $V = J$, $x_c^{(1)} = x_c^{(2)} = 20a$, $s^{(1)} = s^{(2)} = 8a$, $k_0^{(1)} = k_0^{(2)} = \frac{\pi}{2a}$. The single-particle resonance condition, $\epsilon_{k_0^{(i)}} = \Omega$, is fulfilled. Black solid curve: $J_2 = 0$, $\Omega = 0$. Blue dashed curve: $J_2 = 0.2J$, $\Omega = 0.4J$. Green dash-dotted curve: $J_2 = 0.4J$, $\Omega = 0.8J$. Note the finite amount of trapped occupation after scattering.

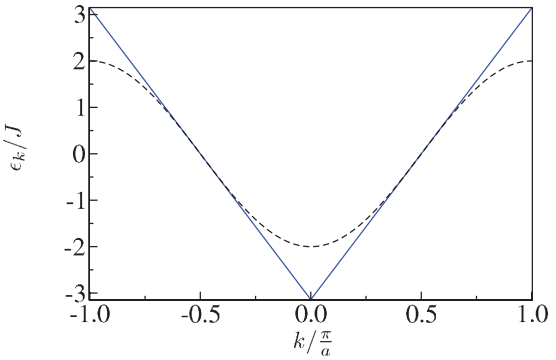

FIG. 3. (Color online) Cosine dispersion $\epsilon_k = -2J\cos(ka)$ (black dashed line) in the first Brillouin zone linearized around $k = \pm\frac{\pi}{2a}$ (blue solid line). Both dispersion relations exhibit cut-offs due to upper and lower band edges that are situated at wave numbers $k = \pm\frac{\pi}{a}$ and $k = 0$, respectively.

that the nonlinear scattering processes will become ineffective so that any excitation of the bound states remains trapped in this state, i.e., we observe a fractional occupation of the TLS's upper level in the long-time limit. Therefore, our results of radiation trapping in Fig. 2 demonstrate that the existence of bound states is not restricted to the special form of the cosine dispersion, which has been analyzed in Eq. (19). Interestingly, the actual amount of trapped radiation depends quite strongly on the value of J_2, i.e., on the dispersion relation. This suggests that a tunable dispersion relation allows for a tunable trapping efficiency.

To further support the above arguments, we display in Fig. 4 the time evolution of the TLS's excited state occupation $\langle n_b(t)\rangle$ for the case of a truncated linear dispersion relation ($k \in [-\pi/a, \pi/a]$) that is constructed by linearizing the cosine-dispersion around $k = \pm\frac{\pi}{2a}$. For $k \geqslant 0$, the resulting dispersion relation is $\epsilon_k = 2J(k - \frac{\pi}{2a})$. In this system, too, we observe radiation trapping that is mediated by nonlinear scattering processes that lead to a nonvanishing occupation of single-particle bound states. In addition, this demonstrates that

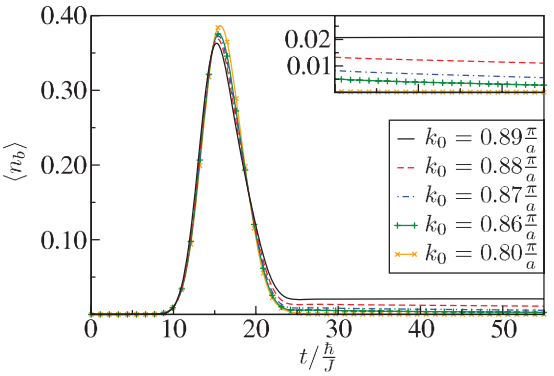

FIG. 4. (Color online) Time evolution of the occupation of the TLS's excited state $\langle n_b\rangle$ for different incoming two-photon wave packets and the truncated linear dispersion relation depicted in Fig. 3. The parameters are (see text for details): $L = 199a$, $x_0 = 100$, $V = J$, $x_c^{(1)} = x_c^{(2)} = 70a$, $s^{(1)} = s^{(2)} = 6a$. The single-particle resonance condition, $\epsilon_{k_0^{(i)}} = \Omega$, is fulfilled in all cases. Note the finite amount of trapped occupation after scattering.

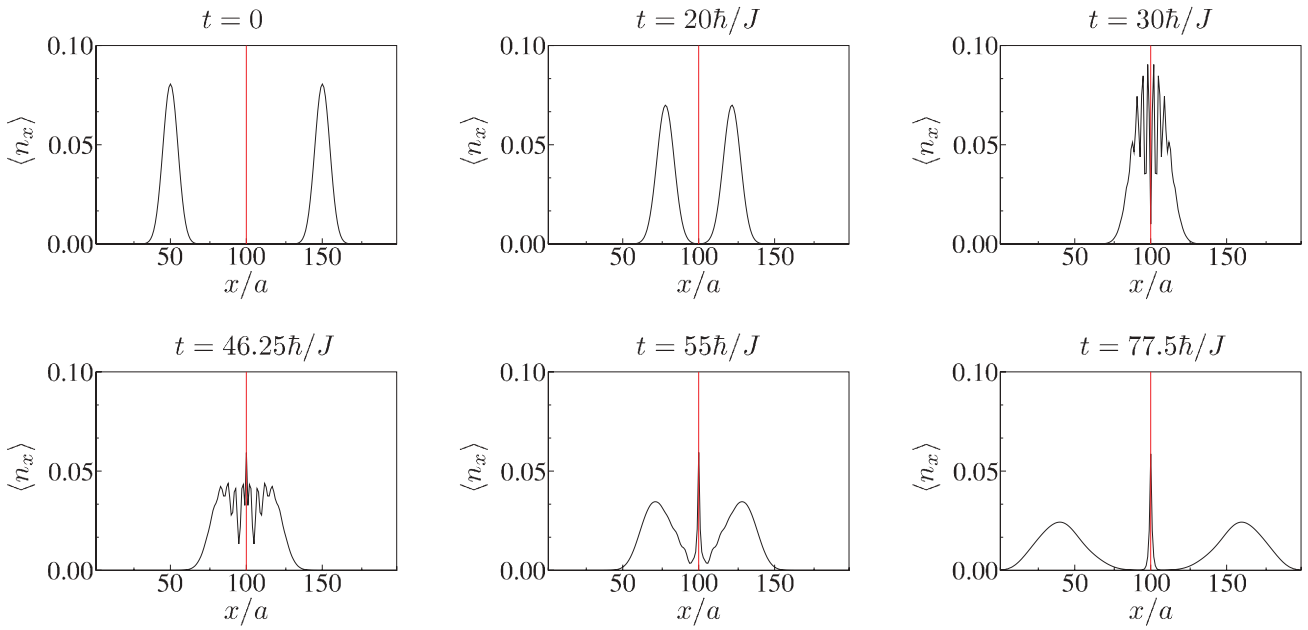

FIG. 5. (Color online) Snapshots of the real-space occupation numbers $\langle n_x \rangle$ of the waveguide sites when two single-photon pulses are launched symmetrically from different sides toward the TLS (cf., the red solid curve in Fig. 6 for the occupation of the TLS). The red line denotes the position of the TLS at $x_0 = 100a$.

linear dispersion relations also lead to single-particle bound states as long as the band edge (or cut-off) is not moved to infinity (cf., Sec. III). Note that $V = J$ in Fig. 4 does not necessarily represent the optimal parameters for radiation trapping, as is the case for the cosine dispersion [33].

We now return to the case of a single TLS that is embedded in a waveguide with cosine-shape dispersion relation. In Fig. 5, we present an alternative route for the excitation of the single-particle bound states via nonlinear multiparticle scattering processes. Specifically, we display snapshots of two single-photon wavepackets that are launched symmetrically from different sides of a waveguide with cosine-shaped dispersion and propagate toward the TLS. When the two wave packets reach the TLS, the quantum interference associated with their scattering at the TLS is clearly visible. After the scattering is complete, an exponentially decaying real-space occupation profile remains around the site of the quantum impurity—the "photonic part" of the (polaritonic) bound state (for the corresponding "atomic part" of the bound state see the red solid curve in Fig. 6). This photon-atom bound state is stable in the long-time limit because it is a true eigenstate of the system (cf., Sec. III).

Very interestingly, by changing the relative initial separations of the pulses with respect to the TLS's position, we obtain a certain degree of control over the amount of trapped radiation as displayed in Fig. 6 (reproduced from Ref. [33]).

In this context, it is instructive to examine the case when one of the two photons is detuned from the atomic resonance. In this case, we launch both photons from the same position and with identical shapes of their wave packets toward the TLS. However, the two wave packets have different momenta and only one fulfills the resonance condition $\Omega = \epsilon_{k=3\pi/4a} = \sqrt{2}$ (see Fig. 7).

This multicolor setup constitutes another way of controlling the amount of trapped radiation. Increasing values of the momentum difference result in an increasing difference in the arrival times of both pulses at the TLS's site due to an increasing group velocity mismatch (recall that we operate with a cosine-shaped dispersion relation). Both effects, detuning and delay, contribute to a lowering of the trapping efficiency relative to the case of two identical photons—and they are clearly not independent: Even if we prepare the initial conditions such that we have a simultaneous arrival of both photons, the different group velocities would still lead to a modified interaction time relative to the case of identical photons. In order to eliminate the effect of pulse delay due

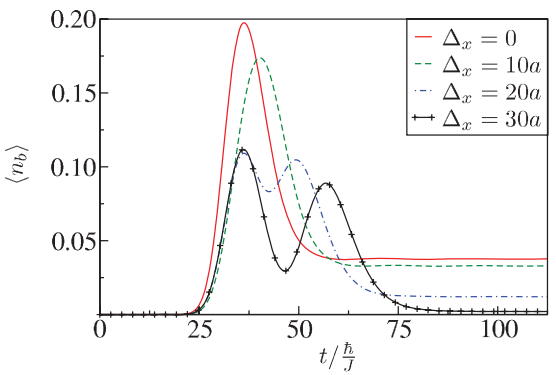

FIG. 6. (Color online) Time evolution of the TLS's excited state occupation $\langle n_b \rangle$ for a setup where two single-photon wave packets are launched with different initial positions relative to the TLS. The parameters are: $L = 199a$, $x_0 = 100a$, $V = J$, $\Omega = \sqrt{2}J$, $s^{(1)} = s^{(2)} = 7a$, $k_0^{(1)} = -k_0^{(2)} = 3\pi/4a$, $x_c^{(1)} = 50a$. The initial position $x_c^{(2)} = 150a + \Delta_x$ of the second single-photon wave packet is varied.

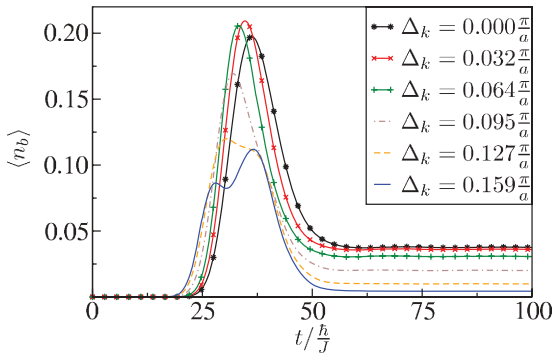

FIG. 7. (Color online) Time evolution of the TLS's excited state occupation $\langle n_b \rangle$ for the interaction with two distinct photons, where only one fulfills the resonance condition prescribed to the cosine-shape dispersion and the other is energetically detuned from the TLS's transition energy Ω. The parameters are: $L = 199a, x_0 = 100a, V = J, \Omega = \sqrt{2}J, s^{(1)} = s^{(2)} = 7a, x_c^{(1)} = x_c^{(2)} = 50a, k_0^{(1)} = 3\pi/4a$. The wave number of the detuned photon, $k_0^{(2)} = k_0^{(1)} - \Delta_k$, is varied by an amount $\hbar\Delta_k$ relative to the resonant photon. For $\Delta_k = 0.159\frac{\pi}{a}$, the detuned photon exhibits a detuning of $0.85J$ with respect to the atomic resonance.

to dispersion, we present analogous results for the case of a linearized dispersion relation (cf., Fig. 3) in Fig. 8.

As a result of the above analysis, we can provide the following physical picture: The existence of single-particle bound states and nonlinear multiparticle scattering processes that result in radiation trapping is a generic feature of a quantum system with discrete levels (for instance, two-level atom or other TLSs), which is coupled to a dispersion relation with a finite bandwidth (band). This can be understood as follows: Once the quantum system is appreciably excited by one of the two (or more) incoming photons, the remaining photons see a saturated and, therefore, modified quantum system and are thus partially scattered into the hitherto unreachable bound states via nonlinear multiparticle scattering processes. At this point, we want to also recall that within the formulation of the problem via Hamiltonian

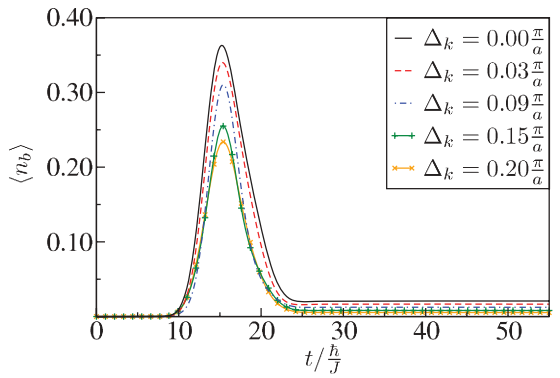

FIG. 8. (Color online) Time evolution of the TLS's excited state occupation $\langle n_b \rangle$ for the interaction with two distinct photons analogous to Fig. 7 but for the linearized dispersion relation (cf. Fig. 3). Parameters: $L = 199a, x_0 = 100a, V = J, \Omega = 2J(k_0 - \pi/2a), s^{(1)} = s^{(2)} = 6a, x_c^{(1)} = x_c^{(2)} = 50a, k_0^{(1)} = k_0 = 0.89\pi/a, k_0^{(2)} = k_0^{(1)} - \Delta_k$. For $\Delta_k = 0.15\pi/a$, the detuned photon exhibits a detuning of $0.94J$ with respect to the atomic resonance.

Eq. (7), the limit $U \to \infty$ represents a "strongly correlated"' system in the language of condensed-matter physics. After the scattering is complete, the photon-atom bound states are again decoupled from the continuum and, thus, cannot decay. As these single-particle bound states are of a polaritonic nature, this implies that a fraction of the radiation remains trapped at the quantum system's position and manifests itself in a fractional occupation of the quantum system's excited level(s).

V. MULTIPARTICLE SCATTERING PROCESSES AND MULTIPLE ATOMIC OCCUPANCIES

Having established the existence and utility of the photon-atom bound state, we turn to a detailed examination of the nonlinear multiparticle scattering processes. This is most easily facilitated by considering the Hamiltonian Eq. (7) and examining the role of the nonlinear on-site interaction term U. At this point, we would like to note that all subsequent computations that involve more than two particles have been carried out with a DMRG approach [43,44].

In a first step, we investigate the role of finite values of U for the scattering of a two-photon wave packet of identical photons. In Fig. 9, we display the time evolution of the atomic excitation $\langle n_b \rangle$ for the scattering of a two-photon wave packet of identical photons for different values of U. This provides a clear demonstration of the role of the nonlinear scattering mechanism induced by the U term: Whereas for $U = 0$ radiation trapping is impossible, increasing values of U lead to an increased trapping efficiency and the limit $U \to \infty$ finally allows for the most efficient trapping.

In the case of $U = 0$, the Hamiltonian Eq. (7) does not contain any nonlinear dependence on the particle number. As a result, it describes an effective single-particle problem so that many-body solutions can be written as direct products of single-particle solutions. In turn, this explains why the photon-atom bound state is inaccessible in this special situation where the atom can absorb infinitely many photons. A single photon with energy in the band is energetically prohibited from reaching a bound state so that the same holds also for direct product states. To further support this statement, we compute the time evolution of the atomic occupation for the scattering

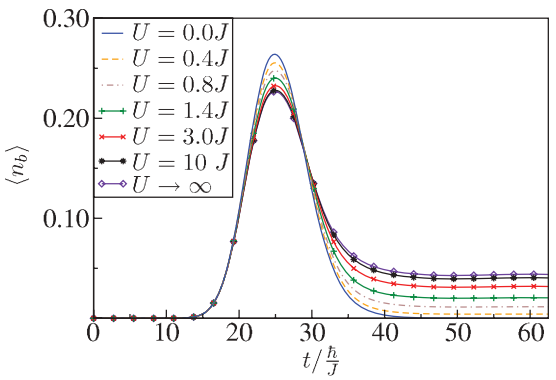

FIG. 9. (Color online) Time evolution of the impurity occupation $\langle n_b \rangle$ for different values of the on-site repulsion U. Parameters: $L = 99a, x_0 = 50a, V = J, \Omega = \sqrt{2}J, s^{(1)} = s^{(2)} = 6a, x_c^{(1)} = x_c^{(2)} = 16a, k_0^{(1)} = k_0^{(1)} = 3\pi/4a$.

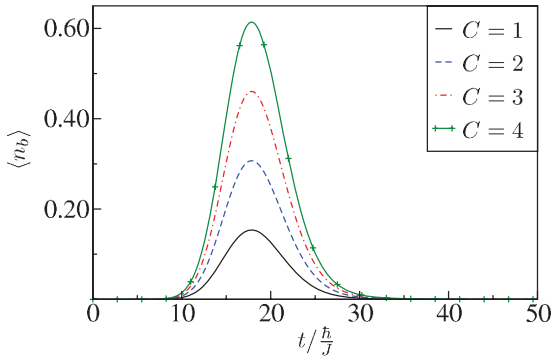

FIG. 10. (Color online) Time evolution of the atomic occupation $\langle n_b \rangle$ for few-photon wave packets of identical photons with different photon numbers C and vanishing on-site interaction $U = 0$. The parameters are: $L = 99a$, $x_0^{(i)} = 50a$, $V = J$, $\Omega = \sqrt{2}J$, $s^{(i)} = 5a$, $x_c^{(i)} = 25a, k_0^{(i)} = 3\pi/4a, i = 1, \ldots, C$. The single-particle resonance condition is fulfilled.

of multiphoton wave packets that contain up to four photons and display the results in Fig. 10. Apparently, also for this case, radiation trapping is absent. Finally, we want to mention that this special case of $U = 0$ corresponds to the (admittedly unphysical) case of an atom with infinitely many degenerate excited levels.

However, we may employ a modification of the Hamiltonian Eq. (7) such that double occupancy of the atomic site is allowed but triple occupancy is strictly forbidden. This modification corresponds to a three-level atom with doubly degenerate excited levels. It is realized by replacing the U term in the Hamiltonian Eq. (7) by

$$U b^\dagger b (b^\dagger b - 1)(b^\dagger b - 2), \tag{20}$$

and taking the limit $U \to \infty$. Based on our above analysis, we expect that a radiation trapping effect is realized only for three or more photons, $C \geqslant 3$. In Fig. 11, we provide the results of corresponding computations for different numbers of photons.

These computations confirm our expectations and thus further support our interpretation regarding the role of nonlinear

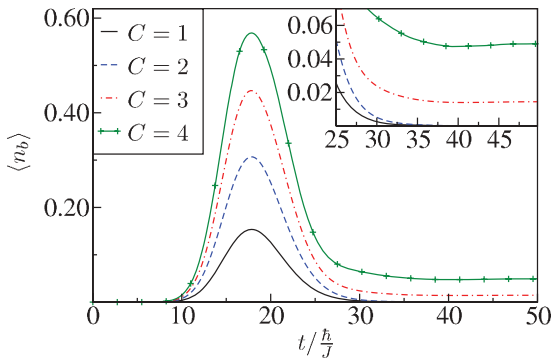

FIG. 11. (Color online) Occupation of the atom's excited level as a function of time in a situation where photon wave packets with different photon numbers C interact with an atom that exhibits a doubly degenerate upper level (cf., Fig. 10 for the relevant parameters).

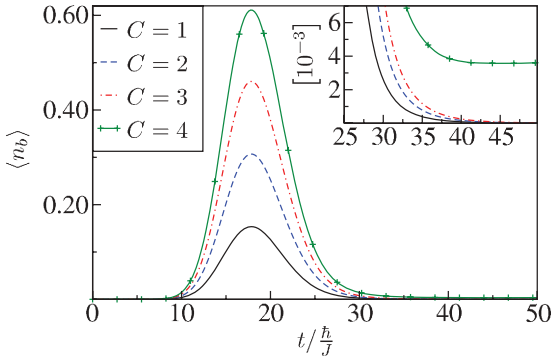

FIG. 12. (Color online) Occupation of the atom's excited level as a function of time in a situation where photon wave packets with different photon numbers C interact with an atom that exhibits a threefold degenerate upper level (cf., Fig. 10 for the relevant parameters).

multiparticle scattering processes. Consequently, if we replace the U term in the Hamiltonian Eq. (7) by

$$U b^\dagger b (b^\dagger b - 1)(b^\dagger b - 2)(b^\dagger b - 3), \tag{21}$$

we realize (again in the limit $U \to \infty$) a four-level system with a threefold degenerate upper level. We depict the results for this situation in Fig. 12 and find that radiation trapping occurs only for photon numbers $C \geqslant 4$ as expected.

The above findings may be compressed into the statement that a saturable absorber is required to allow for nonlinear multiparticle scattering processes with which photon-atom bound states can be reached energetically.

VI. MOMENTUM DISTRIBUTION

As a final element of our analysis, we consider a situation where two photons with different momenta scatter at the TLS with parameters such that the excitation of the bound states is inefficient. Specifically, we choose the coupling $V = 0.8J$, the atomic transition energy $\Omega = 0.1J$, and the photon wave numbers as $k_0^{(1)} = \pi/2a$ and $k_0^{(2)} = 3\pi/4a$. The corresponding single-particle energies in the cosine band, $\epsilon_{\pi/2a} = 0$ and $\epsilon_{3\pi/4a} = \sqrt{2}J$, are, therefore, detuned with respect to the atomic transition. Nevertheless, both photons interact with the atom, which results in a redistribution of the corresponding momenta. We monitor this process with the help of the Fourier transformed amplitudes of the two-photon state vector, Eqs. (14) and (15). In Fig. 13, we display the momentum distribution that corresponds to the part of the full two-photon state vector where the atom is in its ground state. In Fig. 14, we provide the momentum distribution for the atom being in its excited state and one remaining propagating photon. In order to understand the scattering process, both distributions have to be monitored at the same time.

Initially, i.e., before the photons reach the TLS ($t = 0$ and $t = 21.25\hbar/J$), the distribution in Fig. 13 exhibits peaks around the initial wavenumbers according to the initial condition. By the same token, Fig. 14 displays a nil result. In principle, both wave packets would disperse due to the cosine-shaped dispersion relation. However, for the given parameters, this spread is hardly visible while the photons

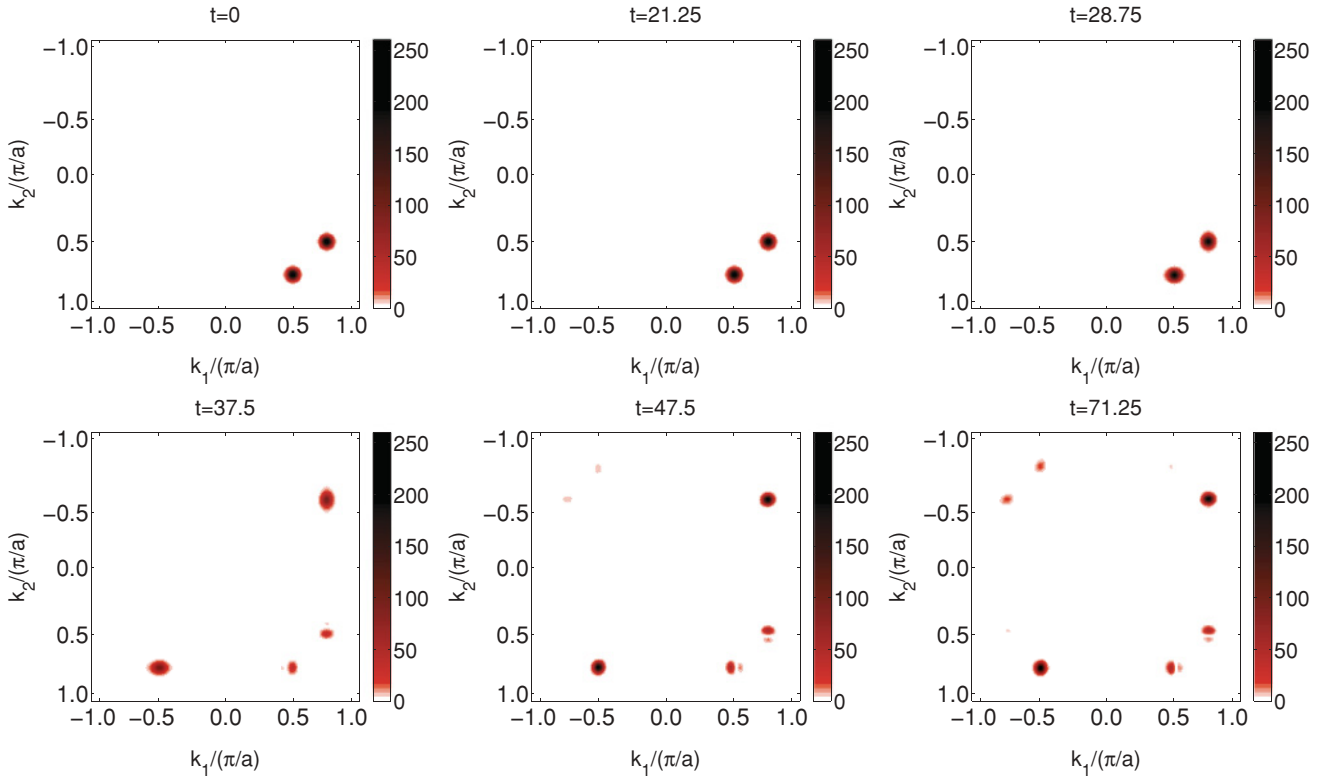

FIG. 13. (Color online) Snapshots of the momentum distribution $|\Phi_{k_1,k_2}|^2$ (in arbitrary units) corresponding to the atom being in its ground state and two propagating photons [cf. Eq. (14)]. Parameters: $L = 199a$, $x_0 = 50a$, $V = 0.8J$, $\Omega = 0.1J$, $s^{(1)} = s^{(2)} = 9a$, $x_c^{(1)} = x_c^{(2)} = 35a$, $k_0^{(1)} = \pi/2a$, $k_0^{(2)} = 3\pi/4a$. The distributions are boson-symmetric with respect to interchanging the wavenumbers k_1 and k_2 at all times (times are given in units of $\hbar/J$).

propagate toward the TLS ($t = 21.25\hbar/J$ in Fig. 13). When the photons approach the impurity ($t = 28.75\hbar/J$), the effect of the different group velocities becomes apparent: The $\frac{\pi}{2a}$-photon arrives first and is less detuned from the TLS than the $\frac{3\pi}{4a}$-photon. Thus, it is partly absorbed by the atom. As a result, the momentum distribution for the atom being

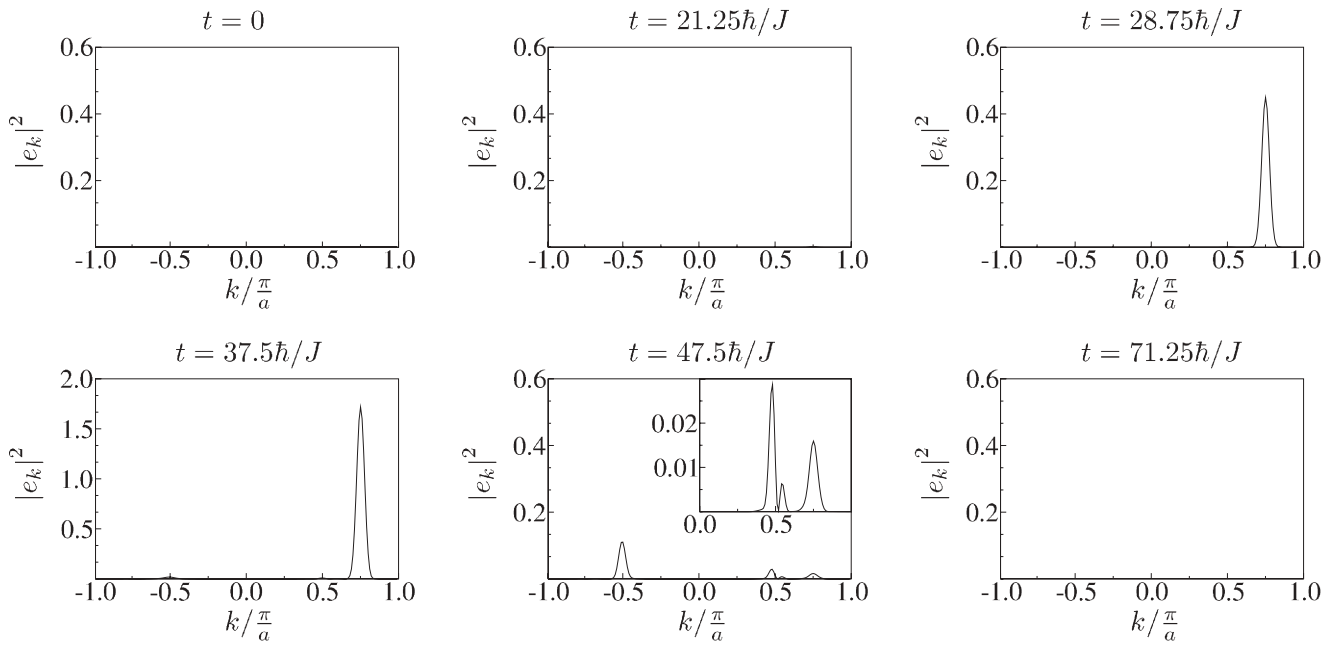

FIG. 14. Snapshots of the momentum distribution $|e_k|^2$ (in arbitrary units) corresponding to the atom being in its excited state and one remaining propagating photon [cf. Eq. (15)]. (Note the differing scale of the y axis at time $t = 37.5\hbar/J$.)

in its ground state is distorted (see $t = 28.75\hbar/J$ and $t = 37.5\hbar/J$ in Fig. 13) and the corresponding distribution of the remaining single photon exhibits contributions around wavenumbers of $\frac{3\pi}{4a}$ (see $t = 28.75\hbar/J$ and $t = 37.5\hbar/J$ in Fig. 14). This demonstrates that it is really the $\frac{\pi}{2a}$-photon that is absorbed and, therefore, the slower $\frac{3\pi}{4a}$-photon continues to propagate. However, together with the re-emission in forward and backward direction of the (partly) absorbed $\frac{\pi}{2a}$-photon ($t = 37.5\hbar/J$), the slow $\frac{3\pi}{4a}$-photon finally reaches the atom ($t = 47.5\hbar/J$), where it is partly absorbed, too. This results in an additional peak of the single-particle momentum distribution $|e_k|^2$ around the wavenumber $\frac{\pi}{2a}$, which now corresponds to the $\frac{3\pi}{4a}$-photon being absorbed with a remaining $\frac{\pi}{2a}$-photon in the waveguide. As the single-particle energy of the $\frac{3\pi}{4a}$-photon is more detuned from the atomic resonance Ω, this fraction of absorbed radiation is smaller as compared to the $\frac{\pi}{2a}$-photon (cf., the heights of the peaks at $t = 28.75\hbar/J$ and $t = 47.5\hbar/J$ in Fig. 14). In addition, at $t = 47.5\hbar/J$, we can also identify the contribution of the re-emitted $\frac{\pi}{2a}$-photon around the wavenumber $-\pi/2a$, which corresponds to the reflected part. After scattering is complete ($t = 71.25\hbar/J$), the atom is in its ground state again so that $|e_k|^2$ vanishes altogether (recall that we have selected the parameters such that no excitation of bound states occurs).

After scattering, $|\Phi_{k_1,k_2}|^2$ exhibits a pattern that corresponds to a final-state vector, which is a superposition of both photons being transmitted, both being reflected, and one photon being transmitted and the other one being reflected. As the shape of the forward propagating parts does not resemble the initial distribution, scattering at the impurity causes a distortion of the initial pulses and, therefore, a nontrivial redistribution of momenta under the constraint of total energy conservation occurs.

VII. CONCLUSION AND OUTLOOK

In conclusion, we have analyzed in detail the role of photon-atom bound states that result when a quantum impurity with two levels is coupled to a low-dimensional waveguiding system. We have demonstrated that these bound states exist whenever the corresponding waveguide dispersions exhibit band edges or cut-offs. These states do not contribute to single-particle scattering scenarios. However, we have shown that when the quantum impurity exhibits a bounded excitation spectrum, it represents a saturable absorber that induces nonlinear multiparticle scattering processes. These processes provide access to the photon-atom bound states. Based on this, we have further shown that these bound states may exert a considerable influence on the photon transport properties. In particular, we have found that it becomes possible to trap radiation at the site of the quantum impurity. Finally, we have demonstrated that the corresponding trapping efficiency can be controlled in a number of ways. This opens up the possibility for realizing novel quantum optical functional elements. For instance, it could be interesting to exploit the tunable dispersion relations for microwave photons that may be realized by superconducting transmission lines with variable bias currents. In these systems, quantum impurities with tunable couplings can be implemented through superconducting qubits. Also, more complex devices such as four-port devices where two transmission lines are coupled by one or several qubits can be implemented. In the optical domain, recent progress regarding the controlled integration of nanodiamonds into fibers [52] suggests that more complex fiber networks are feasible, where nitrogen-vacancy centers in judiciously placed diamonds realize quantum impurities at room temperatures in the sense discussed above.

Furthermore, our results are also of direct relevance for the investigation of so-called Jaynes-Cummings-Hubbard systems, where photons propagate in arrays of coupled cavities where each cavity contains a single TLS. To date, only single-photon transport properties have been studied in such systems [35], and we expect that the photon-atom bound states will lead to considerably different few-photon transport properties and entire quantum simulators may become possible.

Finally, our approach to describe the photon transport can be extended to obtain photon-photon correlations in a similar way as the shot-noise simulations provided in Refs. [53,54].

ACKNOWLEDGMENTS

We express our sincere gratitude to Peter Wölfle for stimulating and fruitful discussions. Further, we acknowledge support by the Deutsche Forschungsgemeinschaft (DFG) and the State of Baden-Württemberg through the DFG-Center for Functional Nanostructures (CFN) within sub-projects A1.2 and B2.10. The PhD student education of P.L. is embedded within the Karlsruhe School of Optics & Photonics (KSOP).

[1] J. Kim, O. Benson, H. Kan, and Y. Yamamoto, Nature (London) **397**, 500 (1999).
[2] P. Michler, A. Kiraz, C. Becher, W. V. Schoenfeld, P. M. Petroff, L. Zhang, E. Hu, and A. Imamoglu, Science **290**, 2282 (2000).
[3] C. Santori, D. Fattal, J. Vuckovic, G. S. Solomon, and Y. Yamamoto, Nature (London) **419**, 594 (2002).
[4] A. Politi, M. J. Cryan, J. G. Rarity, S. Yu, and J. L. O'Brien, Science **320**, 646 (2008).
[5] M. Reischle, C. Kessler, W.-M- Schulz, M. Eichfelder, R. Roßbach, M. Jetter, and P. Michler, Appl. Phys. Lett. **97**, 143513 (2010).
[6] J. Claudon, J. Bleuse, N. S. Malik, M. Bazin, P. Jaffrennou, N. Gregersen, C. Sauvan, P. Lalanne, and J.-M. Gérard, Nat. Photon. **4**, 174 (2010).
[7] C. Santori, D. Fattal, and Y. Yamamoto, *Single-Photon Devices and Applications* (Wiley-VCH, Weinheim, Germany, 2010)
[8] F. Xia, L. Sekaric, and Y. Vlasov, Nature Photon. **1**, 65 (2007).
[9] M. Notomi, E. Kuramochi, and T. Tanabe, Nature Photon. **2**, 741 (2008).
[10] X. Yang, M. Yu, D.-L. Kwong, and C. W. Wong, Phys. Rev. Lett. **102**, 173902 (2009).

[11] T. Yoshie, A. Scherer, J. Hendrickson, G. Khitrova, H. M. Gibbs, G. Rupper, C. Ell, O. B. Shchekin, and D. G. Deppe, Nature (London) **432**, 200 (2004).
[12] G. Khitrova, H. M. Gibbs, M. Kira, S. W. Koch, and A. Scherer, Nat. Phys. **2**, 81 (2006).
[13] K. Hennessy, A. Badolato, M. Winger, D. Gerace, M. Atatüre, S. Gulde, S. Fält, E. L. Hu, and A. Imamoğlu, Nature (London) **445**, 896 (2007).
[14] M. Barth, N. Nüsse, B. Löchel, and O. Benson, Opt. Lett. **34**, 1108 (2009).
[15] P. E. Barclay, C. Santori, K.-M. Fu, R. G. Beausoleil, and O. Painter, Opt. Express **17**, 8081 (2009).
[16] R. Bose, J. F. McMillan, J. Gao, and C. W. Wong, Appl. Phys. Lett. **95**, 131112 (2009).
[17] M. Barth, S. Schietinger, T. Schröder, T. Aichele, and O. Benson, J. Lumin. **130**, 1628 (2010).
[18] L. Frunzio, A. Wallraff, D. Schuster, J. Majer, and R. Schoelkopf, IEEE Trans. Appl. Supercond. **15**, 860 (2005).
[19] A. Wallraff, D. I. Schuster, A. Blais, L. Frunzio, R.-S. Huang, J. Majer, S. Kumar, S. M. Girvin, and R. J. Schoelkopf, Nature (London) **431**, 162 (2004).
[20] M. Hofheinz, E. M. Weig, M. Ansmann, R. C. Bialczak, E. Lucero, M. Neeley, A. D. O'Connell, H. Wang, J. M. Martins, and A. N. Cleland, Nature (London) **454**, 310 (2008).
[21] H. Salehi, A. H. Majedi, and R. R. Mansour, IEEE Trans. Appl. Supercond. **15**, 996 (2005).
[22] T. Niemczyk *et al.*, Nat. Phys. **6**, 772 (2010).
[23] J. L. O'Brien, A. Furusawa, and J. Vučkovic, Nat. Photon. **3**, 687 (2009).
[24] U. Fano, Nuovo Cimento **12**, 154 (1935); Phys. Rev. **124**, 1866 (1961).
[25] J. T. Shen and S. Fan, Opt. Lett. **30**, 2001 (2005).
[26] L. Zhou, Z. R. Gong, Y. X. Liu, C. P. Sun, and F. Nori, Phys. Rev. Lett. **101**, 100501 (2008).
[27] P. Longo, P. Schmitteckert, and K. Busch, J. Opt. A: Pure Appl. Opt. **11**, 114009 (2009).
[28] J. T. Shen and S. Fan, Phys. Rev. A **79**, 023837 (2009).
[29] E. Rephaeli, J. T. Shen, and S. Fan, Phys. Rev. A **82**, 033804 (2010).
[30] J. T. Shen and S. Fan, Phys. Rev. Lett. **98**, 153003 (2007).
[31] J. T. Shen and S. Fan, Phys. Rev. A **76**, 062709 (2007).
[32] T. Shi and C. P. Sun, Phys. Rev. B **79**, 205111 (2009).
[33] P. Longo, P. Schmitteckert, and K. Busch, Phys. Rev. Lett. **104**, 023602 (2010)
[34] D. Witthaut and A. S. Sørensen, New J. Phys. **12**, 043052 (2009).
[35] M. I. Makin, J. H. Cole, C. D. Hill, A. D. Greentree, and L. C. L. Hollenberg, Phys. Rev. A **80**, 043842 (2009).
[36] R. H. Dicke, Phys. Rev. **93**, 99 (1954).
[37] E. T. Jaynes and F. W. Cummings, Proc. IEEE **51**, 89-109 (1963)
[38] K. Busch, S. F. Mingaleev, M. Schillinger, and D. Hermann, J. Phys. Condens. Matter **15**, R1233 (2003).
[39] K. Busch, C. Blum, A. M. Graham, D. Hermann, M. Köhl, P. Mack, and C. Wolff, J. Mod. Opt. **58**, 365 (2011).
[40] C. Moler and C. Van Loan, SIAM Rev. **45**, 3 (2003).
[41] J. Niegemann, L. Tkeshelashvili, and K. Busch, J. Comput. Theor. Nanosci. **4**, 627 (2007).
[42] M. Pototschnig, J. Niegemann, L. Tkeshelashvili, and K. Busch, IEEE Trans. Antennas Propag. **57**, 475 (2009).
[43] S. R. White, Phys. Rev. Lett. **69**, 2863 (1992).
[44] P. Schmitteckert, Phys. Rev. B **70**, 121302(2004).
[45] E. Boulat, H. Saleur, and P. Schmitteckert, Phys. Rev. Lett. **101**, 140601 (2008).
[46] P. Schmitteckert, J. Phys. Conf. Ser. **220**, 012022 (2010).
[47] S. John and T. Quang, Phys. Rev. A **50**, 1764 (1994).
[48] N. Vats, S. John, and K. Busch, Phys. Rev. A **65**, 043808 (2002).
[49] L. Jing, D. Hui, and K. Le Man, Commun. Theor. Phys. **52**, 500 (2009).
[50] S. Longhi, Eur. Phys. J. B **57**, 45 (2007).
[51] G. D. Mahan, *Many-Particle Physics* (Plenum Press, New York, 1981)
[52] T. Schröder, A. W. Schell, G. Kewes, T. Aichele, and O. Benson, Nano Lett. **11**, 198 (2010).
[53] A. Branschädel, E. Boulat, H. Saleur, and P. Schmitteckert, Phys. Rev. Lett. **105**, 146805 (2010).
[54] A. Branschädel, E. Boulat, H. Saleur, and P. Schmitteckert, Phys. Rev. B **82**, 205414 (2010).